GENERAL TRENDS OF THE TOP-MOST SAND UNIT ALONG THE COASTLINE OF SOUTHERN AND CENTRAL ISRAEL

A research report submitted to

The Mediterranean Coastal Cliff Preservation Government Company Ltd.

Submitted by

Yizhaq Makovsky, Adi Neuman, Alexander Surdyaev and Matan Elad

Applied Marine Exploration Laboratory (AMEL)

Charney School of Marine Sciences

University of Haifa

November 2018

Table of contents

סיכום מנהלים

מטרת עבודה זו היא למפות את המגמות הנרחבות (בסקלה של קילומטרים) של שכבת החול העליונה לאורך חופי דרום ומרכז ישראל, ובמידת האפשר לאפיין את החול בשכבה זו בדגש על משמעותו להגנת החוף. אזור המחקר משתרע מגבול עזה בדרום ועד אזור חדרה בצפון, ומקו החוף ועד עומק מים של 30 מ. העבודה מתבססת על מאסף נרחב ככול האפשר של נתונים קיימים.

קבלת הנתונים השונים שנאספו לאורך חופי הארץ מהגופים שונים שמחזיקים בהם היווה אתגר משמעותי במהלך עבודתנו. בנוסף, רבים מהנתונים התקבלו כעותקי נייר או בפורמטים דיגיטליים נחותים, דבר שהקשה על ניתוחם.

בפועל שולבו במאגר הנתונים של המחקר: 451 דגימות סדימנט שנדגמו מהקרקעית בתוך אזור המחקר, ונאספו על ידינו מ 12 דו״חות; 126 לוגים ליתולוגיים, שנאספו מ 6 מקורות ומתוכם 88 לוגים נדגמו בעומקי מים עד 35 מ; ו-11 סקרים סיסמיים בהפרדה גבוהה, עם אורך כולל של כ-4000 ק״מ ומתוכם 1181 ק״מ הם מעומקי מים עד 35 מ. גם בשילוב מאגר הנתונים הנרחב הזה נותרו חורים משמעותיים בכיסוי שטח המחקר, במיוחד בקרבת החוף בחלק הדרומי של שטח זה.

נדגיש ש**כול** הנתונים ששולבו בעבודה זו הגיעו ממקורות ציבוריים פתוחים או אושרו באופן ברור לשימושנו ע״י בעליהם.

שילוב של כלל המדידות של גדלי הגרגר מכול אזור המחקר מראה ששכבת החול העליונה בקרקעית הים מכילה חול דק (0.125 עד 0.25 ממ) ונקי (>95%) עד לעומק מים של כ 30 מ, כ 3 קמ מקו החוף. מעבר לעומק זה יש בקרקעית מעבר חד לסדימנט סילטי-חרסיתי. במספר קטן יחסית של דגימות אחוז החול קטן יותר, מה שמשקף נוכחות של גרגרים גדולים יותר שכנראה מגיעים מחשיפות הכורכר או ריכוזי צדפות בעיקר בקרבת החוף.

התפלגות גדלי הגרגר עם המרחק מהחוף (ועומק המים) מראה שהחציון של גדלי הגרגר של החול (D50) קטן מ-0.23 ממ (±0.3 ממ) בקו החוף ל-0.15 ממ (±0.3 ממ) במרחק של כ-1 ק״מ מהחוף, ועומק מים של כ-15 מ. במרחק ועומקי מים גדולים יותר ה-D50 של החול בקרקעית נשאר קבוע בגודל של כ-0.15 ממ (±0.3 ממ). מדידות של דוגמאות בודדות שנאספו מעומק של כ-1 מ מתחת לקרקעית מציעות שייתכן שמציאותם של גדלי הגרגר שגדולים מ-0.2 ממ מוגבלת רק לקרבת הקרקעית, ובעומק שולטים גדלי הגרגר הקטן יותר גם קרוב (עד לפחות 200 מ) לקו החוף.

תוצאות מיפוי גג הכורכר אינם תואמים לגמרי את המודל של רכסי כורכר שמקבילים בקירוב לקו החוף. מודל זה מתאים בקירוב לחלק הצפוני של אזור המחקר, שם הכורכר חשוף או רדוד (<6 מ) לאורך רוב קו החוף ועד למרחק של לפחות 1 ק״מ ממנו. ברם בחלק הדרומי של אזור המחקר בולט קיומם של גופי כורכר במפלסים שונים בתת הקרקע שאינם תואמים. גג הכורכר באזור זה מצייר אזורים מוגבהים בהם הכורכר חשוף או רדוד, התוחמים עמקים גדולים (עד עומק >30 מ), שאולי תואמים את כיוון מוצאי מערכות הניקוז.

לאורך רוב אזור המחקר שכבת החול העליונה דקה ביותר (עובי <2 מ), והיא עבה יותר רק לאורכה של סדרת עדשות צרות (כ-1 ק״מ רוחב) ומאורכות, המתמשכת במקביל בקירוב לקו החוף ובמרחק של כ-1.5 ק״מ ממנו בדרום כ-2 ק״מ ממנו בצפון. בעדשות אלה שכבת החול העליונה מתעבה במקצת ומגיעה לעובי >4 מ ועד לכ-12 מ באזורים מצומצמים בין תל-אביב לאשדוד.

נפח החול הכולל בשכבה העליונה באזור המחקר הוא כ-700 מיליון קוב, שמתוכם כ-450 מיליון קוב מרוכזים בתוך סדרת העדשות. תפוצת גדלי הגרגר מעידים שרובו המכריע של החול בשכבה זו מתאפיין ב-D50 של כ-0.15 ממ (ובוודאי קטן מ-0.2 ממ).

עבודה זו לא עסקה בשכבות חול עמוקות יותר שבוודאי נמצאות בין שכבת החול העליונה וגג הכורכר בדרום אזור המחקר. העיסוק בשכבות אלה נמצא מחוץ למטרותינו המוגדרות. מעט מאוד נתונים קיימים על אפיון שכבות אלה, ונתונים אלה בד״כ לא היו זמינים לנו. ברם, ניצול שכבות עמוקות אלה, באם ימצאו מתאימות, ידרוש הסרה מסיבית של שכבות הקרקעית, עובדה שקרוב לוודאי הופכת אותן ללא רלבנטיות.

Executive summary

This work aims to map the regional (km-scale) trends of the top most sand layer along the coast of southern and central Israel, and where possible to characterize the sand in this layer focusing on its relevance for coastal preservation. The research area stretches from the Gaza border in the south to Hadera region in the north, and from the coastline to a water depth of 30 m. This work is based on a comprehensive, as much as possible, collection of existing datasets.

Obtaining the various datasets, collected along the Israeli coast, from the entities holding them constituted a major challenge in course of this work. Additionally, many of the datasets were obtained as paper copies or in vintage digital formats, which hampered their interpretation.

In total the research database combined: 451 seafloor sediment samples from the research area, from 12 reports; 126 lithological logs, from 6 surveys, out of which 88 logs were sampled at water depths ≤35 m; and 11 high resolution seismic surveys, with a total running profiled length of ~4,000 km and 1181 km of these were acquired at water depths ≤35 m. This pervasive database still leaves significant holes in the coverage of the research area, particularly near the coastline in its southern part.

We emphasize that <u>all</u> the data utilized in this work either were obtained from open public sources, or were explicitly approved by the proprietors.

The grain size measurements from the entire research area combined show that the top most sand layer contains, at the seafloor, fine (0.125-0.25 mm) clean (usually >95%) sand to a water depth of ~30 m, ~3 km from the coastline. Beyond that depth, there is a sharp transition at the seafloor to silty-clayey sediments. In a relatively small number of samples the sand fraction is smaller, which reflects the presence of larger grains that probably arrive from primarily nearshore Kurkar outcrops or shell concentrations.

The distribution of the grain sizes with the distance from the coastline (and water depth) shows that the median grain sizes (D50) decreases from 0.23±0.03 mm near the coastline to 0.15±0.03 mm at a distance of ~1 km from the coastline, and a water depth of ~15 m. At greater distances and water depths the sand D50 remains approximately constant at 0.15±0.03 mm. Measurements of a few samples, which were collected at a depth of 1 m below the seafloor, suggest that the presence of D50 >0.2 mm is limited to the proximity of the seafloor, and at depth the small grain sizes are more abundant closer (at least to a distance of 200 m) to the coastline.

The top of Kurkar mapping results do not fully accord with the model of a series of Kurkar ridges, sub-parallel to the coastline. This model is approximately adequate for the northern part of the research area, where the Kurkar is exposed or shallowly (<6 m) buried along most of the coastline and to a distance of at least 1 km from it. However, in the southern part of the research area Kurkar bodies are prominently found in different and not correlated sub-surface levels. The top of Kurkar in that area draws elevated areas of exposed or shallowly buried Kurkar, that bound relatively large basins (to depths >30 m) aligned possibly along drainage outlets.

Along most of the research area the top most sand layer is very thin (<2 m thickness), and it is thicker only along a narrow (~1 km wide) set of slivers, that stretch sub-parallel to the coastline at a distance of ~1.5 km and ~2 km from it in the south and north respectively. Within these slivers the top most sand layer thickens slightly, reaching thicknesses of >4 m and up to ~12 m in small areas between Tel-Aviv and Ashdod.

The total sand volume in the top most layer in the research area is ~$700x10^6$ m^3, out of which ~$450x10^6$ m^3 are concentrated in the sand slivers. The distribution of grain sizes reveals that the majority of the sand in this layer is characterized with D50 of ~0.15 mm (and certainly less than 0.2 mm).

This work did not investigate deeper sand layers that probably exist between the top most sand layer and the top of Kurkar in the southern part of the research area. The investigation of these layers is outside the scope of this work. Very little data exist, which could characterize these layers, and these data were generally not available to us. However, exploitation of these deeper layers, if found adequate, would require a massive removal of the seafloor layers, which probably renders such exploitation irrelevant.

Scope of work

The purpose of is work is to map the regional trends (several kilometers resolution) of the upper sub-sea sand layer along the Mediterranean coast of Israel, and where possible to characterize the sand in this layer. This work is focused on the relevance of the sand in this layer for coastal preservation. The area of interest spans the shallow water strip from the Gaza border to Hadera region and from the coastline to a water depth of 30 m. This work is to be carried out based on a comprehensive, as much as possible, collection of existing datasets, which were collected by the different public and private organizations over the years.

Introduction

The near surface levels of the southern to central Israel coastal zone is composed of the Late-Pleistocene to Holocene Kurkar Group - Hefer Formation, composed primarily of alternating units of calcareous sandstones (Kurkar), eolianites, reddish clayey-silty paleosol (Hamra), dark swamp clays, marine silts and clays, regosol, and loose sands (e.g. Gvirtzmanet al., 1984; Gvirtzman et al., 1997; Frechen et al., 2002; Mauz et al., 2013). On land, the Kurkar forms a northward converging sub-parallel set of ridges (figure 1), composed of interbedded amalgamations of units of Kurkar, Hamra and other lithologies with different Late Pleistocene ages (e.g. Neev et al., 1987; Gvirtzman et al., 1998; Almagor et al., 2000; Engelmann, 2001; Frechen et al., 2001, 2002; Sivan and Porat, 2004; Porat et al., 2004; Mauz et al., 2013). These units are partly correlated along much of the coastline (Gvirtzman et al., 1998). The western of these ridges is intermittently aligned with the coastline (figure 1), and is actively eroding by waves action to form a coastal cliff along parts of the Israeli coast (e.g. Neev et al., 1987; Nir, 1982, 1984, 1992; Almagor et al., 2000; Katz et al., 2007; Mauz et al., 2013; Kattz and Mushkin, 2013). This onshore geological structure is suggested to continue westwards based on offshore sub-bottom profiling and drill holes (e.g. Neev et al., 1987; Gvirtzman et al., 1997). Accordingly, a northward converging set of sub-parallel drowned and buried ridges (figure 1), with their crests outcropping to form bathymetric ridges, were outlined across the continental shelf of Israel through bathymetric and sub-bottom profiling and suggested to be Kurkar ridges corresponding to the onshore ones (e.g. Neev et al., 1987; Nir, 1984; Almagor et al., 2000).

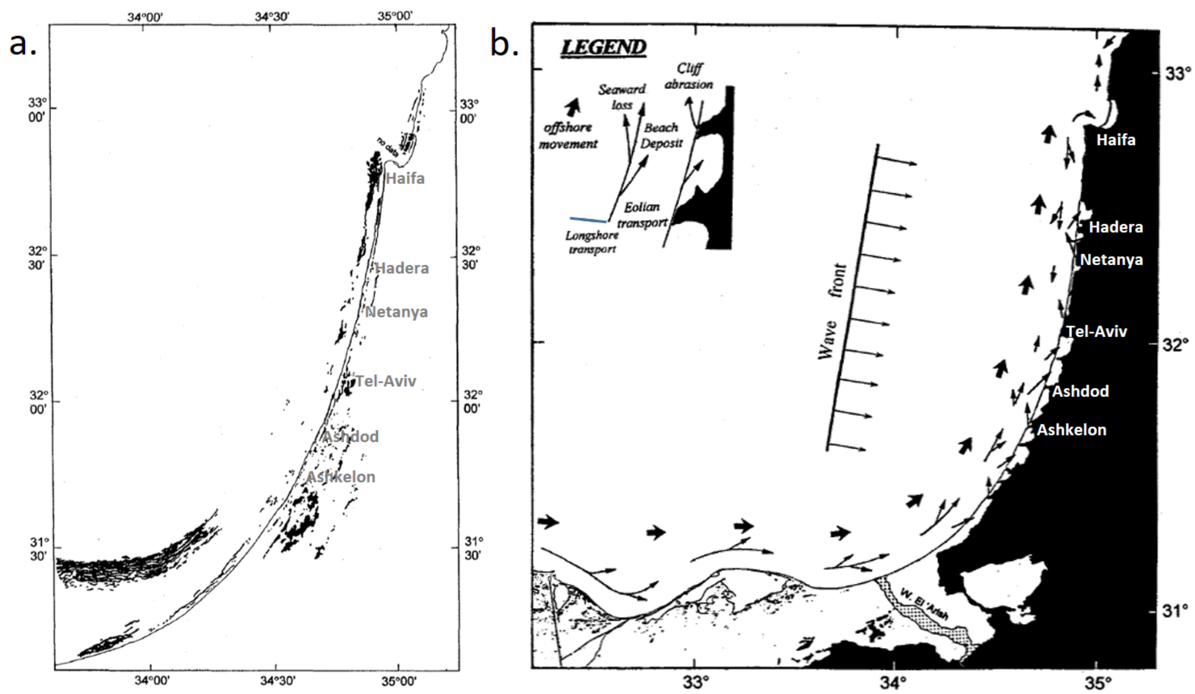

Figure 1. (a.) Kurkar outcrops on the continental shelf and coastal plain of Israel. (b.) Offshore and longshore transport of suspended Nile Sand along the southeastern Mediterranean shelf and littoral zone, with onshore dune fields shown in white. (From Almagor et al. (2000).)

A prominent, up to 0.5 km wide, belt of up to 25 m tall buried Kurkar ridges (to be named here “the 30 m Ridge”; figure 2) extends along the coastline of Israel (figure 1), with its crests emerging up to 10 m above the surrounding seafloor (Almagor et al., 2000). Opposite southern Israel it lies 2-3 km from the coastline at water depths of 20 to 30 m, while opposite central Israel it lies 3 to 4 km from the coastline at water depths of 30 to 50 m and becomes increasingly continuous northward. In central Israel, terrestrial clayey swamp deposits and Paleosols (primarily Hamra) are deposited in the basin between the coastline and the 30 m ridges, uncomfortably overlaid by a mid- to late- Holocene unconsolidated marine sand unit (e.g. Nir, 1984; Almagor et al., 2000; Sivan et al., 2004; Mauz et al., 2013; Shtienberg et al., 2016; Goff et al., 2018; figures 2, 3). In the vicinity of the 30 m ridge, where the effect of the base of storm waves declines, the sand unit pinches out and transitions to a clayey-silt marine layer (figure 2; e.g. Nir, 1984; Neev et al., 1987; Golik et al., 1999; Almagor et al., 2000; Almogi-Labin, 2012). This silt layer thickens westwards, overlying Kurkar, terrestrial and marine sandy units. In southern Israel, the section contains significantly greater sand content and the top-most sand layer is underlain by other sandy units of various compositions, separated in places by intercalations of terrestrial clayey paleosols (Avital, 2002; DHV, 2011; figure 4). On the west, the top sand layer transitions to silty and clayey sand units. Sand in the top-most layer is generally clean and well sorted, with the modal grain size usually between 0.11-0.3 mm (e.g. Almagor et al., 2000; Sivan and Almogi, 1999; Hyams-Kaphzan et al., 2008; Almogi-Labin et al., 2012; Almagor and Perath, 2012). The grain size slightly decreases with distance from the coast and with the northing. However, due to a northward increase in skeletal carbonate content, the coastal sand appears to become coarser northwards (Almagor et al., 2000; Golik. 2002; and references therein). This study focuses on mapping this top-most sand layer.

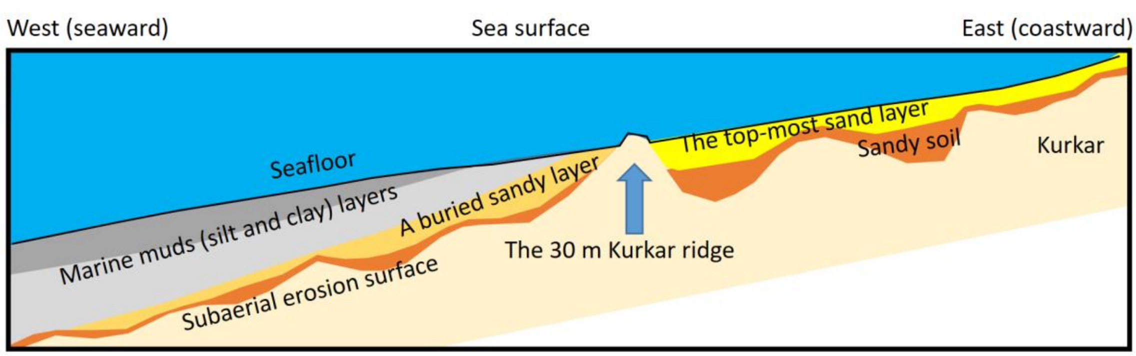

Figure 2. A schematic profile across the inner to middle Mediterranean shelf of Israel, showing the erosional surface at the top of the Kurkar unit and the field relations of ‘soft’ sediment units overlaying it (after Nir (1984)). The top-most sand unit and the ’30 m Kurkar ridge’ (see text) are highlighted (blue).

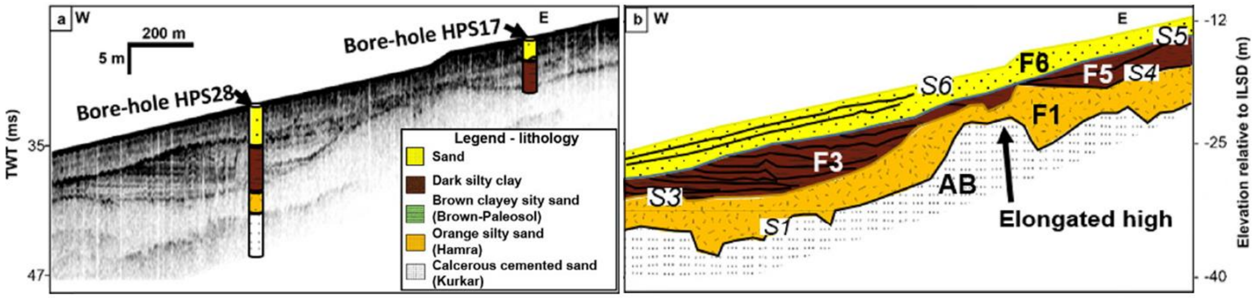

Figure 3. A borehole controlled seismic-lithological profile across the inner shelf offshore Hadera, at the northern bound of the study area, showing the field relations of the near surface sediment units (adapted from Shtienberg et al. (2016)). This section shows a ~2-3 m thick westward transitional top-most sand unit (yellow), overlying on an unconformity at the top of the terrestrial swamp deposits (brown) and Hamra (orange). The latter fill topographic lows in the Top-Kurkar diagenetic/erosional surface. Shtienberg et al. (2016) mapping served as the northern anchor for this study's interpretation and mapping.

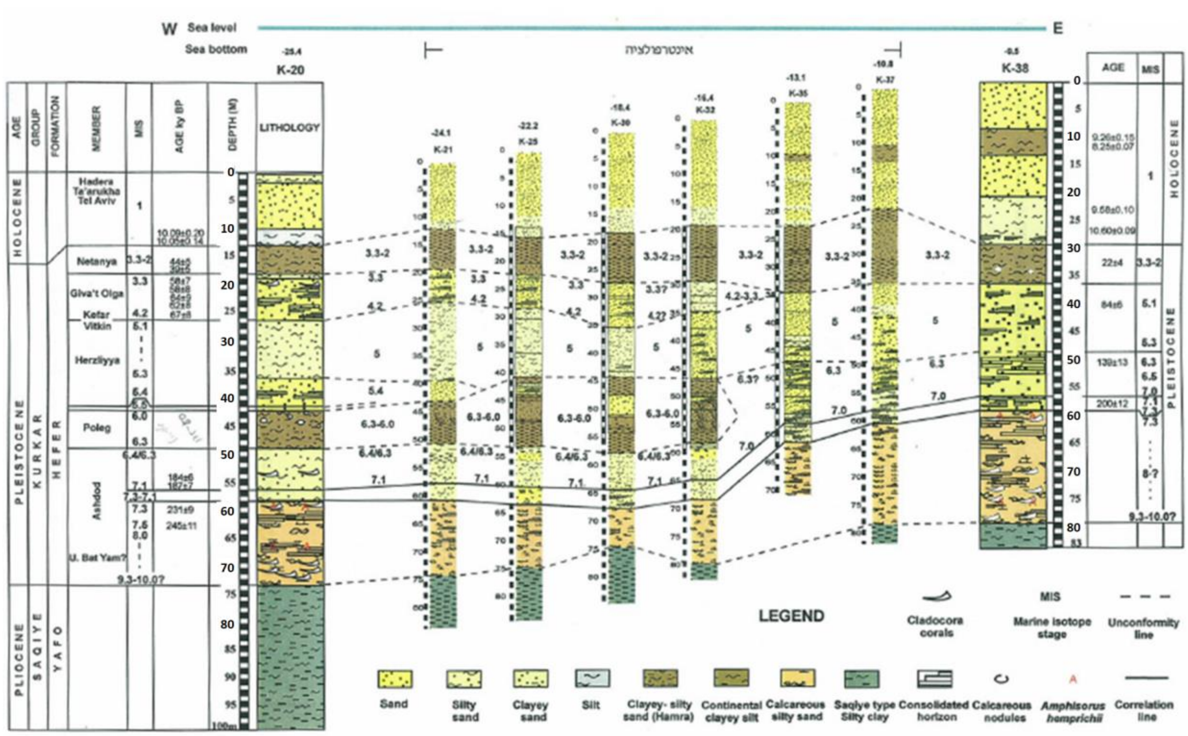

Figure 4. A multi-borehole time and space lithological correlation of the Plio-Quaternary sections of across the inner shelf offshore Ashkelon, at the southern bound of the study area (from Avital (2002)). The correlation is based on U-Th, OSL/IRSL and ^{14}C ages, lithology and indicative foraminifera and macrofauna abundance is the K-20 and K-38 cores (Avital, 2002; Porat et al., 2003); and geotechnical characteristics across the full set of cores (Soil and Roads Laboratory, 1993). This section is showing the field relations of near surface sediment units. This section has lower lithological definition. Yet, it shows a much greater predominance of sand then figures 3, and a much less distinct top-most sand unit (UMS), partly bounded at its base by a terrestrial clayey-silty sand unit. The boreholes of this section were as anchors for this study's interpretation and mapping.

The top-most sand layer is maintained by a balance between sand sources and sinks. The primary source of the Mediterranean coastal sands of Israel is from the Nile and they are generally transported by regional counter-clock currents along the inner continental shelf (figure 1b), as shown by mineralogical studies (e.g. Emery and Neev, 1960; Pomerancblum, 1966; Nir 1984); pre-1964 visual and chemical observations of Nilotic flood plumes (e.g. Hect, 1964; Inman and Jankins, 1984); and seafloor scours and the distribution of coal particles (Golik, 1993); and direct current estimations (e.g. Emery and Neev, 1960; Almagor et al., 2000 and references threin). In a pioneering effort Katz and Crouvi (2018) have directly monitored over one year the sediments transport over a 25 m deep seafloor, 2 km offshore Hadera, measuring a greatly variable, but consistently northwards sediment transport. In the nearshore, usually to 5 to 6 m water depth, sand is transported primarily by wave action and waves-generated currents (Emery and Neev, 1960; Almagor et al., 2000; Zviely et al., 2007; Almagor and Perath, 2012). At the short term sand gradually builds up along the coasts in the summer, while large volumes of sand are mobilized to and from the coasts by winter storms and associated currents (Almagor et al., 2000, and references therein). These currents depend on the direction and to lesser extent on the period of wave's impingement with respect to the arcuate coastline, resulting with converging-transport nodal points (e.g. Goldsmith and Golik, 1980). Sand accumulation-erosion pattern across coastal obstacles shows that the long-term net nodal point is located approximately in front of Tel-Aviv, corresponding to waves traveling at an azimuth of ~281° along the long axis of the Eastern Mediterranean Sea (e.g. Emery and Neev, 1960; Goldsmith and Golik, 1980; Shoshany et al., 1996). Thus, south of Tel Aviv the net nearshore sand transport is northwards, while to the north (between Tel Aviv and Haifa) the net transport is southwards. The estimated net long-shore transport of sand gradually decreases along the Israeli coastline from ~450,000 m^3/yr in Ashquelon, to ~100,000 m^3/yr in Tel Aviv and ~85,000 m^3/yr in Haifa (Emery and Neev, 1960; Golik and Rosen, 1999; Perlin and Kit, 1999; Almagor et al., 2000; Golik, 2002; Zviely et al., 2007). With the contribution of sand by coastal drainage or wind being negligible, the only other important sand is supplied by the long-term erosion of the coastal Kurkar cliffs and coastline (e.g. Emery and Neev, 1960; Almagor et al., 2000). Long-term estimates of sand contribution by cliff erosion vary between 50,000 m^3/yr (Nir, 1984) and ~200,000 m^3/yr (Perath, 1982; Almagor et al., 2000). Most recently, Mushkin et al. (2016) estimated the rate of cliff erosion at 45,000 m^3/yr based on repeated LIDAR observations between 2006 and 2015. They noted that sand contribution amounts to ~50% of the sand transport rate in central Israel, and therefore cliff retreat mitigation efforts may lead to sand deficit and increased coastal erosion. Sand loss is estimated to occur primarily through seaward sand transport and distribution over the shelf and basin, but also as by wind driven landward sand migration, sand mining and accumulation by various obstacles constructed along the coastline (e.g. Almagor et al., 2000). Until the construction and operation of Aswan Dam, the Nile River was the sand source, while since then the Nile Delta and Northern Sinai sand reserves continue the supply of sand (Almagor et al., 2000; Golik, 2002). Zviely et al. (2007) note that the net sediment transport rate at Haifa Bay did not change appreciably over the preceding 75 years, despite the potential impact of natural or anthropogenic changes.

Several integrated attempts were made to evaluate the sand resources along the Mediterranean coastline of Israel. However, due to the technical difficulty in shallow water geophysical mapping and profiling, the nearshore top-most sand layer was only partially imaged and mapped. Recently this layer was investigated by several focused studies, associated mostly with local development projects. This study aims at combine the range of newly available dataset and re-evaluate the structure and composition of the top-most sand layer.

Data and Methodology

At the center of this study is the collection of various datasets available, their co-registration into a common GIS database and workbench, and the interpretation of these data with respect to the top-most sand layer. The interpretation is aimed to delineate the compositional variability of the top-most sand layer in terms of median grain size (D50) and sand fraction, and map the depth to the base of the upper sand layer and top of Kurkar based on seismic sections correlated with lithological logs. Data incorporation and analysis were carried out at the Applied Marine Exploration Laboratory, University of Haifa, utilizing in conjunction Paradigm multi survey and well-databases Project desktop and ArcGIS database.

An important part of this study was in the collection of the different datasets, many of which are restricted by the possessors of these data based on proprietorship or other reasons. All datasets incorporated into this study were obtained by proprietors/possessors permission, or from official publicly available sources (e.g. official governmental web sites). Thus, some of the important vintage datasets have only been found as figures in paper copy report, while others may have been partly or entirely lost.

The nearshore datasets available are mostly dense surveys or traverses, focused on small areas. A few regional datasets, primarily the 1997-1998 Artificial Islands survey, cover pervasive areas along and across the Israeli shelf, but have little coverage at the shallow (<20 m) water depths. To exploit the regional datasets the analysis was expanded to deeper water (generally out to 35 m water depth), to reach and sometimes cross the 30 m Kurkar ridge belt. This verified the pinch-out of the top-most sand layer and established the identification of undelaying units, allowing connecting between the localized datasets. Yet, major data gaps exist at water depths <20 m along the coastline, which needed to be filled by long-range interpolations.

a. Sediments characterization data

These data include grain-size distribution parameters, used to obtain the grain-size median (D50) and sand fraction. Table 1 summarizes the datasets obtained and compiled by us. Sampling strategies of these datasets varied between surface collection of sediments by divers or grabs, and extraction of short cores. In either case, all datasets, except to dataset 10 in Table 1, sampled only the surficial level of the sand layer. The different datasets were obtained with variable quality indicators: from tables and pervasive plots, or digital databases, of analyzed values coupled with a full report of the acquisition and analysis procedures; through low quality paper-copies of grain-size distribution graphs; to D50 values plotted on a map. In addition, the laboratories and analysis methodologies varied, from sieves to laser diffraction mastersizer. In some cases the fines (<0.062 mm) and/or coarse (>2 mm) fractions were omitted, and needed to be conjured by us. The D50 and sand fraction values were extracted from the various datasets, and were registered with respect to the sampling positions in an ArcGIS database (figure 5a). In some cases, the positions was manually digitized off map figures or conjured based on the available description. In total 451 samples were processed and incorporated into the database.

Table 1. The sources of sediment characterization samples incorporated in this study.

	Source	**Area**	**# of samples**		**Sampling method**	**Sampling years**
			In database	**Depth <35 m**		
1	Stadler et al. (1996)	Ashkelon	47	47	Bed samples	1989
2	Sivan and Almogi-Labin (1999)	5 sections along the inner shelf	35	35	Diving & collection	1996-1999
3	Almogi-Labin et al. (2009)	Cores along the middle shelf	28	26	Short (0.15-0.3 m) cores	2003-2008
4	Almogi-Labin et al. (2012)	9 sections along the shelf	29	25	Grab/box-corer	2011
5	Almagor et al. (1998)	Across the shelf	27	13	Vibrocorer sampled @ 0-0.4 m	1997-1998
6	Levin et al. (2011)	Netanya	70	70	Seafloor sampling	1996
7	Mivdaka (2013)	Herzeliya	141	141	Seafloor sampling	2013
8	Spier and Ben Yosef (2016a)	Ashkelon	14	14	0.25 m cores, collected by divers	2016
9	Spier and Ben Yosef (2016b)	Hadera	5	5	0.25 m cores, collected by divers	2016
10	Jan De Nul Group (2017)	Ashdod	22	22	Piston core sampled @ 0.9-1.5 m	2017
11	Tzadok (2018) a	Ashdod	17	17	Repeated analysis of #10: Piston core sampled @ 0.9-1.5 m	2017
12	Tzadok (2018) b	Ashdod	16	16	Short cores, 0.1-0.3 m	2017

b. Lithological logs

Lithological logs interpreted based on boreholes, cores and CPT measurements were used for correlating and interpreting the seismic sections. The lithological log datasets incorporated in this study are listed in Table 2. The lithological interpretations were incorporated into this study as obtained from the sources listed. These interpretations vary in their precision. For example, the definition of 'Sand' in one source may correspond to 'Fine silty sand' in the other. Yet, no re-interpretation of lithologies from the original data was attempted here, mainly because the full scope of the data were usually not available. The lithological log depths and descriptions were digitized and co-registered with sampling positions in ArcGIS database (figure 5b). In addition, these data were loaded into Paradigm software as lithological well logs and tops, creating a separate well database for each of the sources listed in Table 2. These logs were then combined and displayed on the relevant seismic sections during their interpretation. Depth to time conversion of these logs was approximated with a constant velocity of 1500 m/sec. In total 126 lithological logs were incorporated in this project, out of which 88 are at water depth <35 m.

Table 2. The lithological logs incorporated in this study.

	Source	Area	# of samples		Sampling method	Sampling years
			In database	Depth <35 m		
1	Nir (1977), Shtienberg et al. (2016)	Hadera	7	7	Water-Jet drilling	1977
2	Israel Electrical Company, Shtienberg et al. (2016)	Hadera	41	41	Piston cores	1982
3	Israel Electrical Company, Avital (2002)	Ashkelon	24	24	Boreholes	1993
4	Port of Ashdod North Development – 1995, DHV (2011)	Ashdod	21	21	Boreholes	1993-1995
5	Port of Ashdod Container Terminal Development, DHV (2011)	Ashdod	10	10	Boreholes	2010
6	Artificial Islands survey: Fugro Engineers BV (1998), Almagor et al. (1998)	Across the shelf	34	11	Vibrocore	1997-1998
7		Across the shelf	21	11	CPT	1997-1998
8		Across the shelf	16	11	Other	1997-1998

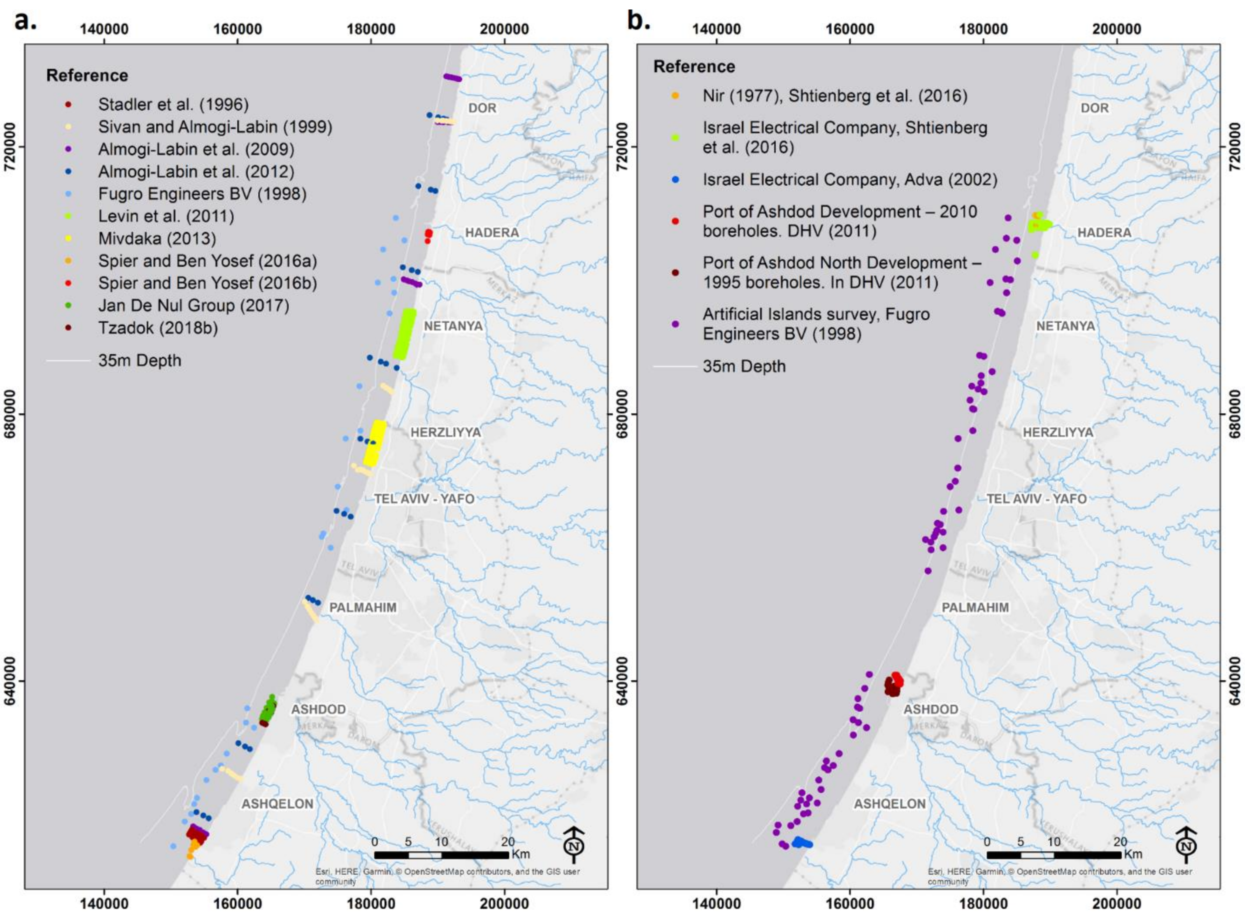

Figure 5. Distribution maps of sediment samples (a.) and lithological logs (b.) incorporated into the study database, color coded by the different data sources listed (Tables 1 and 2). The 35 m water depth contour is marked in white.

c. Bathymetry

Several bathymetric datasets were available for this survey, widely ranging in their acquisition times, resolution and expanse. However, matching the different datasets was not straightforward. The different datasets incorporated into this survey were all referenced to a single 5 m bathymetric grid digitized from a vintage contour map of the Israeli inner shelf produced by Oceana by single beam surveying. Scaling to time (for working with the geophysical time data) was performed with a velocity of 1500 m/sec. This referencing facilitated the common interpretation of the different database. It does not affect the accuracy of the final products, produced as maps of isopach thickness with respect to the seafloor. The coastline is defined in this study by the *Survey of Israel* official coastline, as was provided by MCCP.

Outcrops of Kurkar at the seafloor were automatically picked from the bathymetric grid based on the seafloor gradient exceeding 2° (figure 6), then edited manually to omit erroneous picking. In addition, Kurkar outcrop outlines at shallow water depths were picked based on coloration in Google Earth images and the proximity of onshore cliff outcrops (figure 6). These were incorporated into both the ArcGIS and

Paradigm databases, providing zero-thickness control to both the Kurkar depth and top-most sand layer thickness.

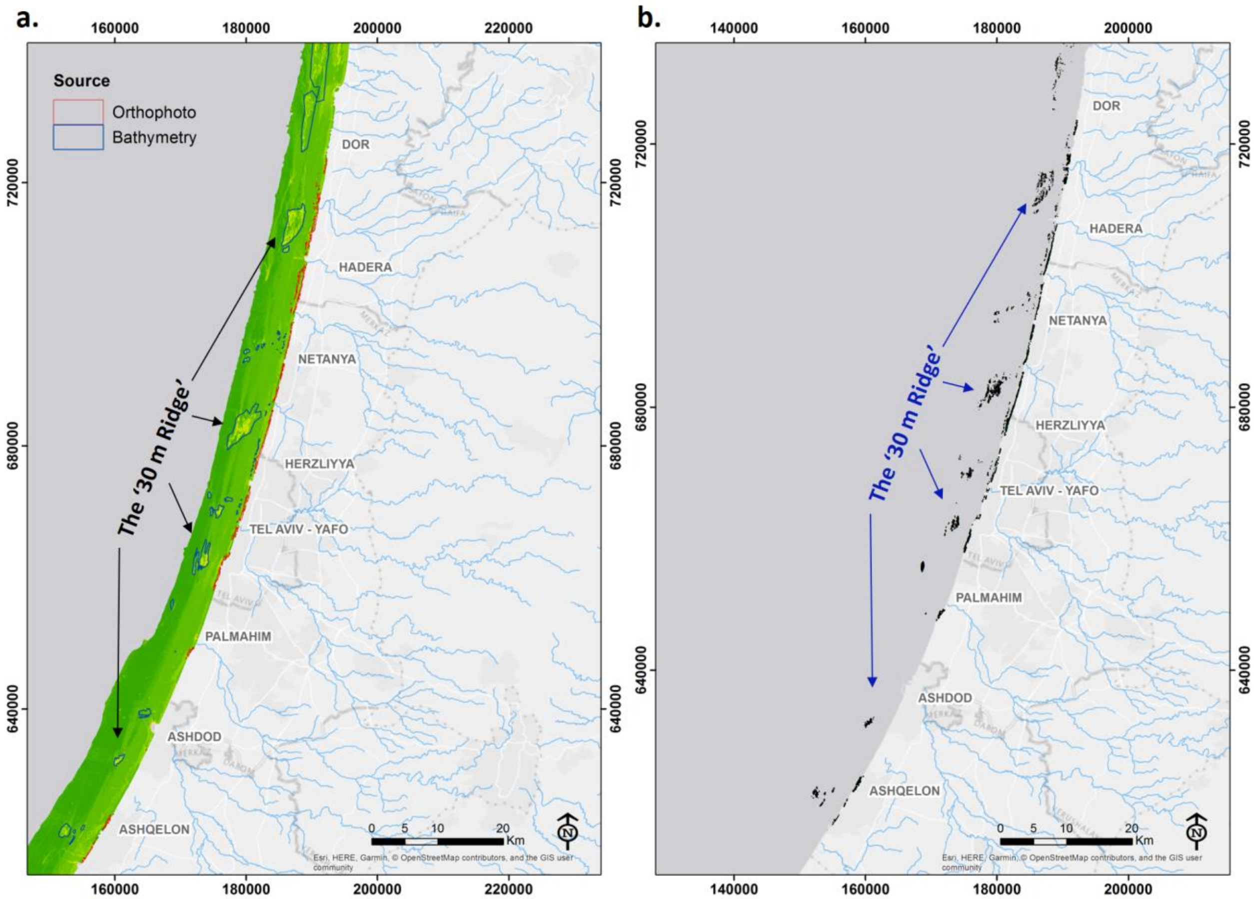

Figure 6. (a.) A gradient map of the bathymetric grid used in this study, overlaid by manually picked bounds of Kurkar outcrops. This map highlights the change in seafloor gradient occurring across the '30 m ridge', and the high gradients associated with the Kurkar outcrops. Blue polygons bound the Kurkar outcrops observed in the bathymetry, and the red polygons mark the Kurkar maps manually picked from Google Earth along the coastline. (b.) The zero-thickness picks of Kurkar outcrops, as picked and used in this study.

d. Seismic sub-bottom profiles

Eleven 2D high (decimetres) resolution sub-bottom profiling surveys, totalling ~4000 km, were integrated into the study databases (Table 3; figure 7). Six of these surveys are focused on limited nearshore areas. The other five surveys, particularly the Artificial Islands sub-bottom survey, extend over large areas of the Israeli shelf. However, the latter offer little coverage of the shallow (<20 m) water area. Seven of the surveys were acquired using various (primarily ~2-7 kHz) Chirp sub-bottom profilers, offering a high-resolution image of the seafloor, but limited signal continuity and penetration. The other four surveys were acquired with University of Haifa GeoMarine Survey System 0.5-2.5 kHz sparker system. This system offers a bit limited imaging at the vicinity (<1 m) of the seafloor, but significantly improved signal continuity and penetration. The combination of data acquired with the two systems provided important insights for this study. Unfortunately, for two of the most important datasets, namely the Artificial Islands and Gaash surveys, only degraded versions of the data were obtained. It seems that the original datasets were lost, and the only copies retrieved are decimated 8-bit data preserved in a vintage interpretation workstation at the Geophysical Institute of Israel. In addition, wrong sampling rates found in the headers of some of the vintage data were identified and redefined.

Table 3. The seismic surveys incorporated in this study.

	Survey	Operator	Years of acquisition	Total profiled km		Profiling device
				In database	Depth <35 m	
1	Gas Pipe	Oceana	1993	498	178	Chirp
2	Gaash*	?	1990s	35	35	Chirp
3	INGL Gas Pipe	Oceana	2003	191	19	Chirp
4	Artificial Islands*	IOLR	1997-1998	1800	590	Chirp
5	IOLR Hadera 2007	IOLR	2007	30	30	Chirp
6	IOLR Hadera 2013	IOLR	2013	34	34	Chirp
7	EDT Herzliya	EDT	2013	161	161	Chirp
8	IOLR Palmahim	IOLR	2009	76	76	Sparker
9	IOLR Nitzanim	IOLR	2012	21	21	Sparker
10	DMG Netanya	DMG-IOLR	2013	408	26	Sparker
11	DMG Israel Shelf	DMG-IOLR	2015	706	11	Sparker

* Only a degraded vintage interpretation workstation version of the data was obtained by us.

e. Joint interpretation and mapping

Joint interpretation of all loaded surveys and lithological logs was carried out in Paradigm Project desktop. The seafloor reflections were picked for all profile segments used in this study, providing the reference for isopach thickness calculations. Two sub-bottom surfaces, the base of the top-most sand unit and the top of the Kurkar (the base of soft sediments), were picked on all profiles on which they could be identified. Picking was initiated in the vicinity of the lithological logs positions, where the units were identified, and was recursively examined against existing logs. The isopach thicknesses of the two surfaces were then calculated by subtraction of the seafloor reflection times on a line-by-line basis, and scaling to depth with a velocity of 1500 m/sec. The resulting isopach picks were then merged with the zero-thickness picks derived for the bathymetric and nearshore Kurkar outcrops. Isopach thickness maps were interpolated across the entire analysis area (exceeding the 35 m depth contour) using Paradigm Adaptive Fitting algorithm (Axis deviation = 13; B/A axis ratio = 3), and gridded at 25 m cells. The final isopach maps were created by cutting the previous maps to the defined study area, limited between the coastline and the generalized outline of the 30 m water depth contour.

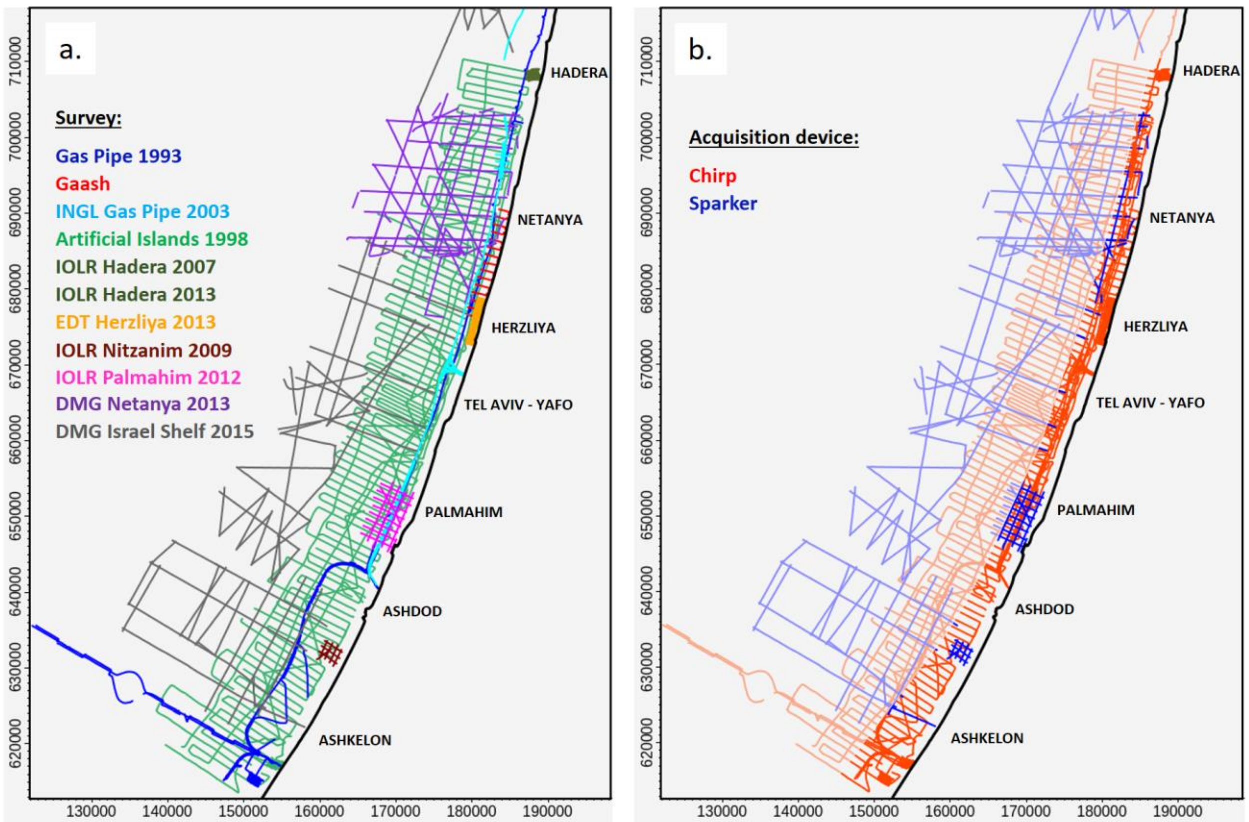

Figure 7. Profile lines of the sub-bottom surveys incorporated into the database in this study (table 3), color coded according to the survey name (a.) and the acquisition device (b). The profile lines at water depths >35 m are faded in (b). While the middle shelf is extensively covered by the incorporated surveys, not much of the nearshore is covered.

Results

a. Sediment characterization

The distribution of D50 values (figure 8a) and grain size fractions (figure 9) in the study area demonstrates the predominance of fine (0.125-0.25 mm) sand at the seafloor in water depths of up to 25 m along the entire coastline of southern and central Israel. To the west, at 30 to 35 m water depth east of the 30 m ridge, there is a relatively abrupt and distinct transition to fine (0.009-0.016 mm) and clayey (0.005-0.008 mm) silt. A higher definition inspection of the D50 values (figure 8b) reveals that the sand is well sorted and clean, predominantly smaller size (0.125-0.18) fine sand. Lower sand fractions (between 80-95 %) measured within the sand belt correspond generally with coarser D50 values, reaching coarse sand and even granules. These are presumably associated with large particles shedding off Kurkar outcrops, predominantly along the coastline in the northern part of the study area. However, these anomalies may have also been associated with insufficient separation of aggregates during some of the laboratory measurements, as suggested for example by the unusual consistency of relatively high values in the Levin et al. (2011) dataset (see table 1 and figure 5), sampled along the Netanya coastline.

We observe general uniformity of measured D50 values and sand fractions, probable D50 measurement inconsistencies and large data gaps along the study area. Taken together, these render impractical the interpolation of useful robust maps of D50 and sand fraction for the study area.

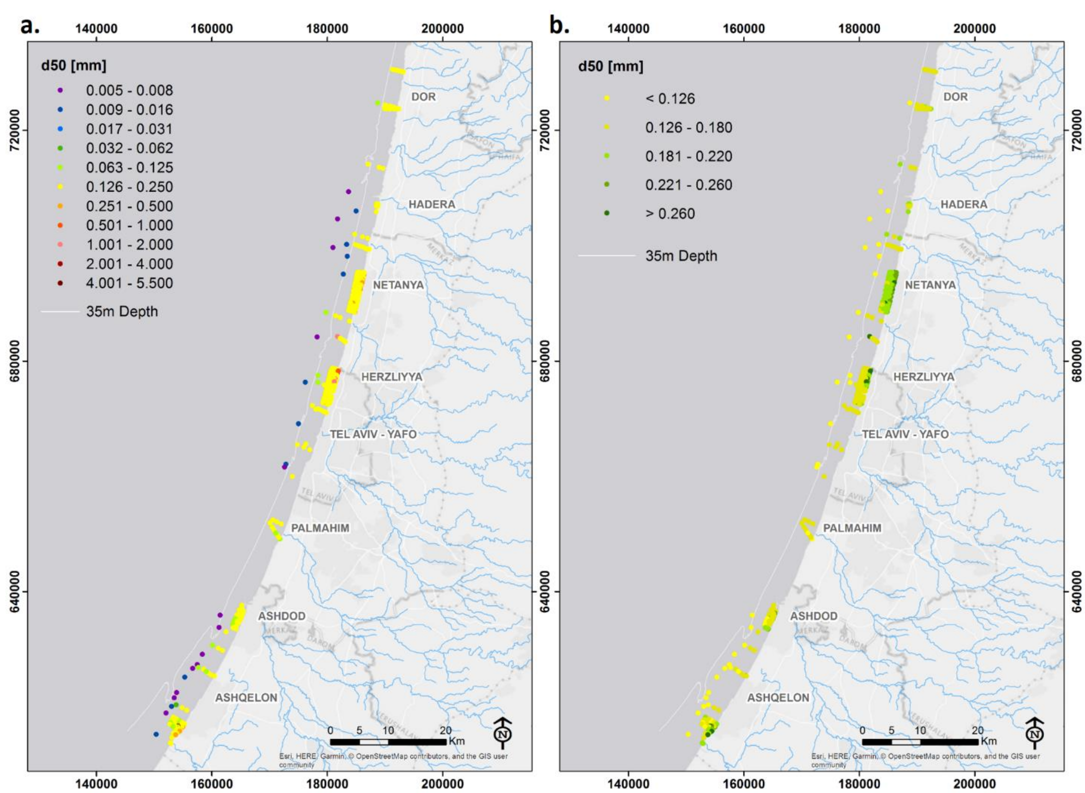

Figure 8. The distribution of measured sediments grain size D50 along the study area, plotted according to Wentworth (1922) grain size scale (a) and with a higher definition of the 0.126-0.260 mm grain sizes.

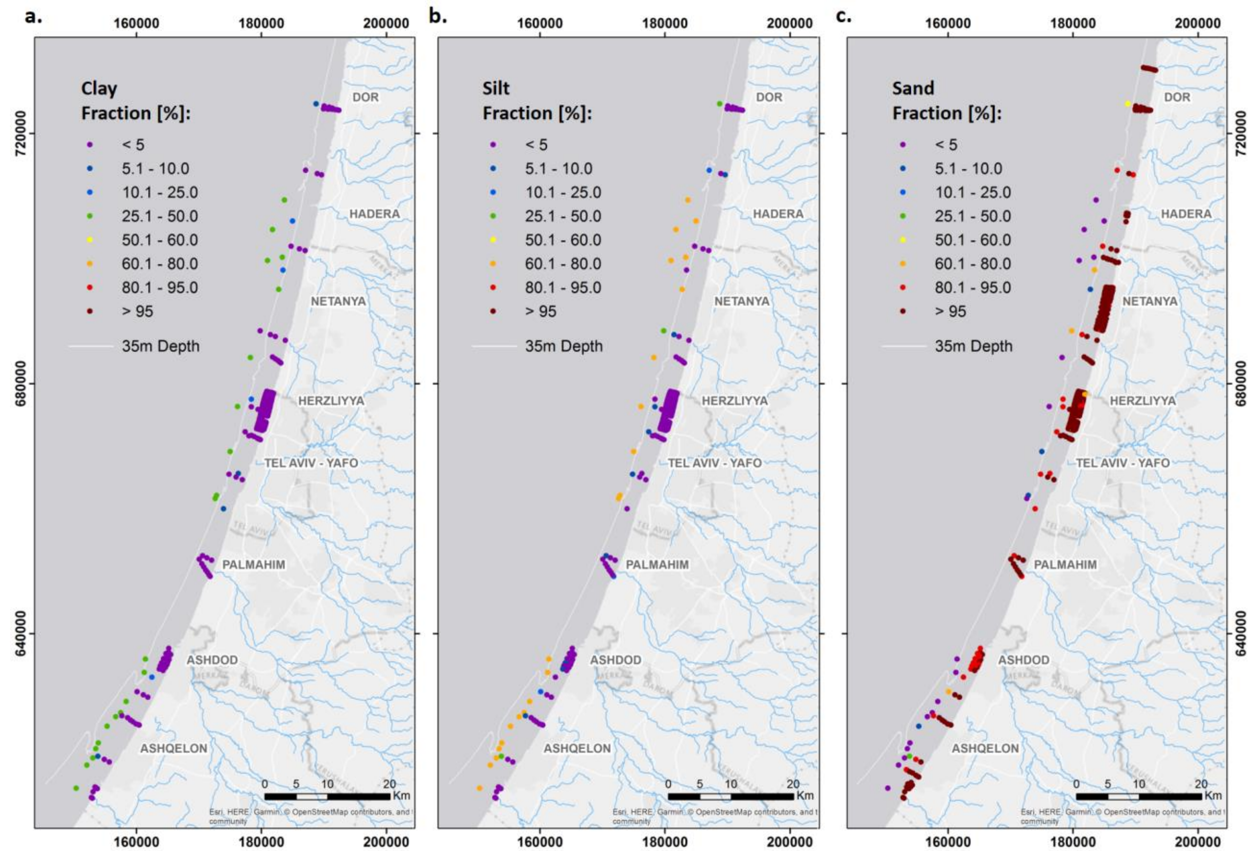

Figure 9. The distribution of measured sediments clay (a.) silt (b.) and sand (c.) fractions along the study area.

Scatter plots of the D50 measurements (figure 10) verify that there is a considerable (~0.1 mm) variation between measurements within most datasets, and between the different datasets. Yet, a clear trend is observed of D50 values with distance from the coastline (and water depth; figure 10a). The D50 values are highest, ~0.23±0.03, near the coastline and decrease to ~0.15±0.03 at a distance of ~1 km and water depth of ~15 m. These results are in agreement with previous publications (e.g. Almagor and Perath, 2012; and references therein). Farther offshore the D50 values remain approximately constant, until the edge of the sand belt at a depth of ~30 m, ~3 km offshore. There the seafloor composition changes to predominantly silt and clay. Tzadok (2018a) compared samples he collected at the seafloor (0.1-0.3 m sediment depth; to ~15 m water depth and ~1 km from the coastline) with repeated analysis of samples collected from a sediment depth of 0.9-1.5 m (Jan De Nul Group, 2017; figure 10a), and argued that the surface measurements represent only a thin veneer at the seafloor and the sand is finer at deeper levels within the top-most sand layer. Placing the measurements in the broader context shows the Tzadok (2018b) surface measurements are relatively high, but also that the D50 values of the samples collected deeper in the sediment are consistent with the D50 values found at >1 km distance from the coastline (and water depth >15 m). There appears to be a minor (~0.03 mm) northward increase of the D50 values sampled at water depths >15 m along the coastline (figure 10b). However, it is not clear how significant this trend is. Examination of the temporal changes of the D50 values (figure 10d,e) appear to suggest an increase of the grain size in the summer and decrease in the winter, as well as an increase of the grain size with the years since 1999. However, considering the small number of samples for which the date is available and particularly samples collected in the winter, the different water depths and geographical positions sampled in the different times, as well as possible inconsistency in the laboratory analyses, these temporal trends are highly questionable.

Figure 10. Scatter plots of the available D50 measurements with respect to distance from the coastline (a), position along the coastline (b) and (c), sampling month (d), and sampling year (e). Only measurements for which the sampling date is available are included in (d) and (e). (e.) Note that the data were sampled at the seafloor (<0.5 m sediments depth). The exception are Jan De Nul Group (2017) samples, and Tzadok (2018a) repeated analysis the same, which were collected at sediments depths of 0.9-1.5 m. The measurements are generally color coded according to the data sources (table 1), while in (c) the measurements are color coded by the seafloor water depth (box on the left of (c)). Conceptual trends are marked on the plots (gray dashed lines) where relevant (see discussion in the text).

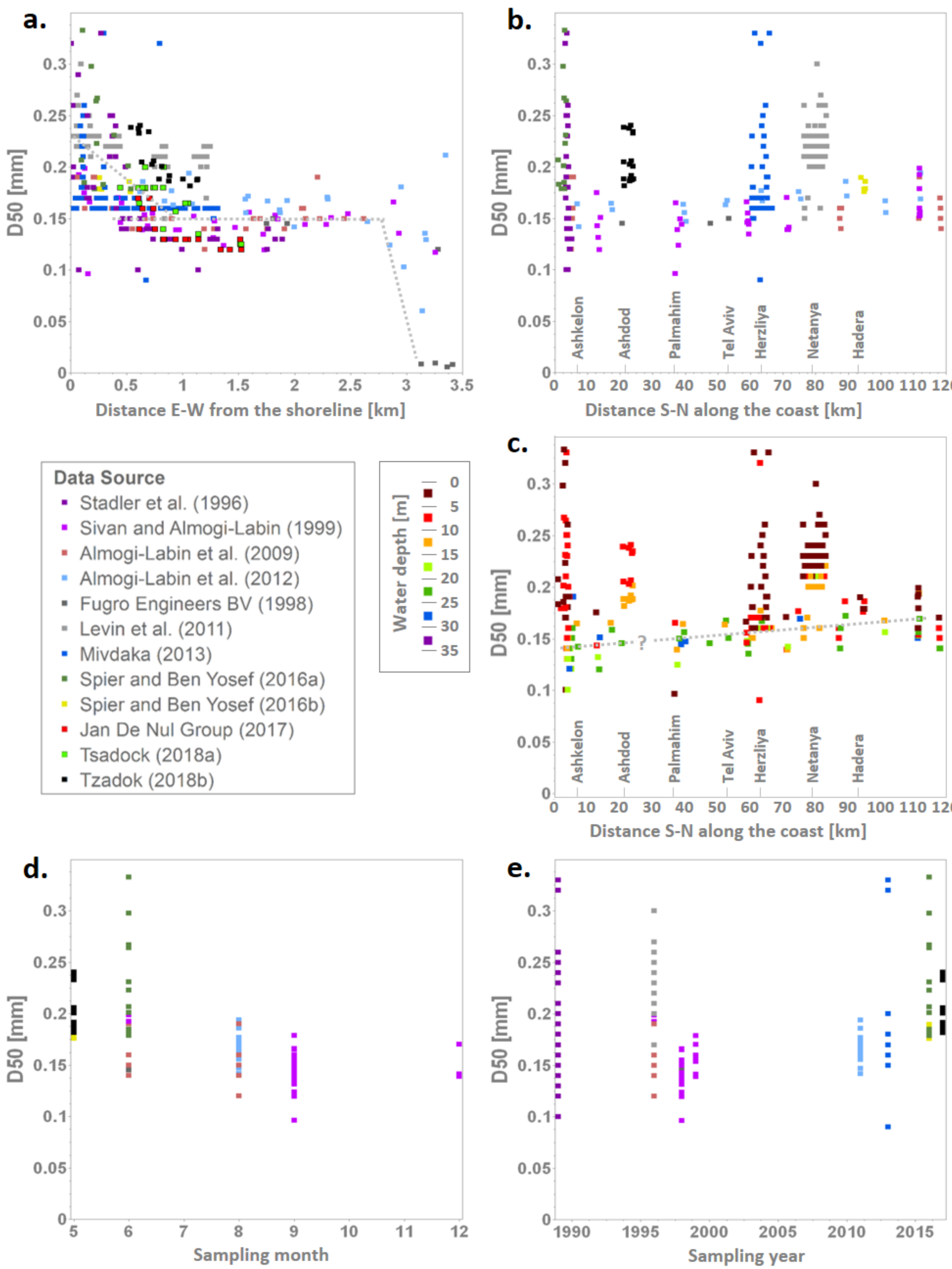

a.
b.
c.
d.
e.
D50 [mm]
Distance E-W from the shoreline [km]
Distance S-N along the coast [km]
Ashkelon
Ashdod
Palmahim
Tel Aviv
Herzliya
Netanya
Hadera
Data Source
Stadler et al. (1996)
Sivan and Almogi-Labin (1999)
Almogi-Labin et al. (2009)
Almogi-Labin et al. (2012)
Fugro Engineers BV (1998)
Levin et al. (2011)
Mivdaka (2013)
Spier and Ben Yosef (2016a)
Spier and Ben Yosef (2016b)
Jan De Nul Group (2017)
Tsadock (2018a)
Tzadok (2018b)
Water depth [m]
Sampling month
Sampling year

b. Seismic identification of the top of Kurkar and top-most sand unit

Interpretations of the seismic sections are anchored on previous studies (e.g. figures 3,4) and the lithology log markers incorporated into the Paradigm database:

1. The top of Kurkar:

The top of Kurkar is usually characterized as a distinct high-amplitude jagged band of reflections, corresponding with the outcrops of offshore Kurkar ridges and constituting the acoustic basement for high-resolution (predominantly Chirp) seismic profiles (e.g. Neev et al., 1966; Almagor et al., 2000; figure 11, 12). However, between Kurkar ridges in relief troughs filled by terrestrial sediments, the latter are commonly imaged as high amplitude reflections and the top of Kurkar may appear as weak and discontinuous set of reflections (e.g. Almagor et al., 2000; figures 3, 11, 12). Moreover, in the nearshore the Kurkar reflection may be entirely masked by the seafloor reflection (e.g. figure 11). Some of the lithology logs constrained the presence of deeply buried Kurkar where the available seismic profiles could not image it (e.g. figures 4, 11). In contrast to the Chirp profiles, the Sparker profiles (e.g. figures 14, 15) provide a significantly deeper penetration, imaging the details and context of the buried Kurkar. These profiles reveal that the offshore Kurkar forms a series of distinct irregular bodies, situated sometimes at different levels. The connection between these bodies may indeed be ambiguous, implying that the concept of a single 'top of Kurkar surface' is not accurate. Thus, along much of the survey area, and particularly where the Kurkar is relatively deeply buried, the interpretation and mapping of the top of Kurkar are conceptual, providing some first order estimate to the depth to a possible hard rock surface.

2. The base of the top-most sand unit:

Shtienberg et al. (2016) characterized the top-most sand unit in the northern bound of the study area as a seismically transparent unit, bounded at its base by a distinct reflection that truncates the layering of the undelaying terrestrial units (figure 3). Correlation of the Chirp seismic profiles with the available lithological logs (e.g. figures 11-15) indicates the presence of distinct reflectivity at the base of the top-most sand unit along much of the nearshore in the study area. Albeit, in some places there is some ambiguity in identifying the correct reflectivity band (e.g. figure 11,12). A greater difficulty is associated with defining the western termination of the top-most sand unit, at its transition towards the middle shelf clayey silt unit (e.g. figure 2). The sediments characterization samples (figures 8, 9) reveal that this transition occurs somewhat to the west of the 30 m Kurkar ridge, ~2.5 km from the coastline at water depths of 25-30 m. This change in sediment grain-size correlates with the transitional westward appearance of layered reflectivity just beneath the seafloor (e.g. figures 11, 14, 15). The base of the top-most sand unit is interpreted in this study to cut arbitrarily upwards across the onset of the layered reflectivity and terminate at the seafloor.

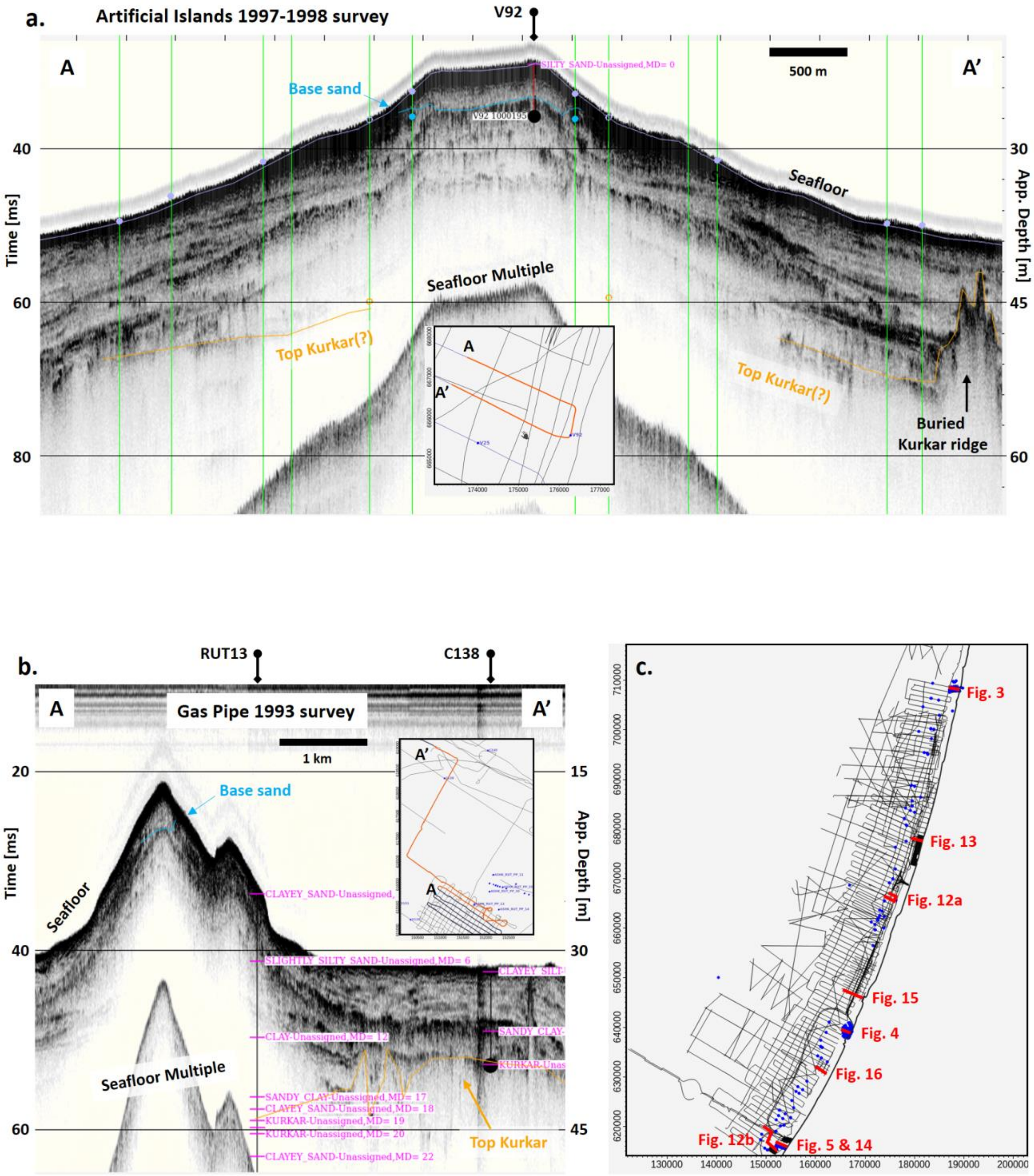

Figure 11. Chirp sub-bottom profiles of the Artificial Islands 1997-1998 (a) and Gas Pipe 1993 (b) surveys, and the correlation of the interpretation surfaces with the lithological logs. (c.) A location figure for all the seismic and lithological section figures presented in this report (labeled).

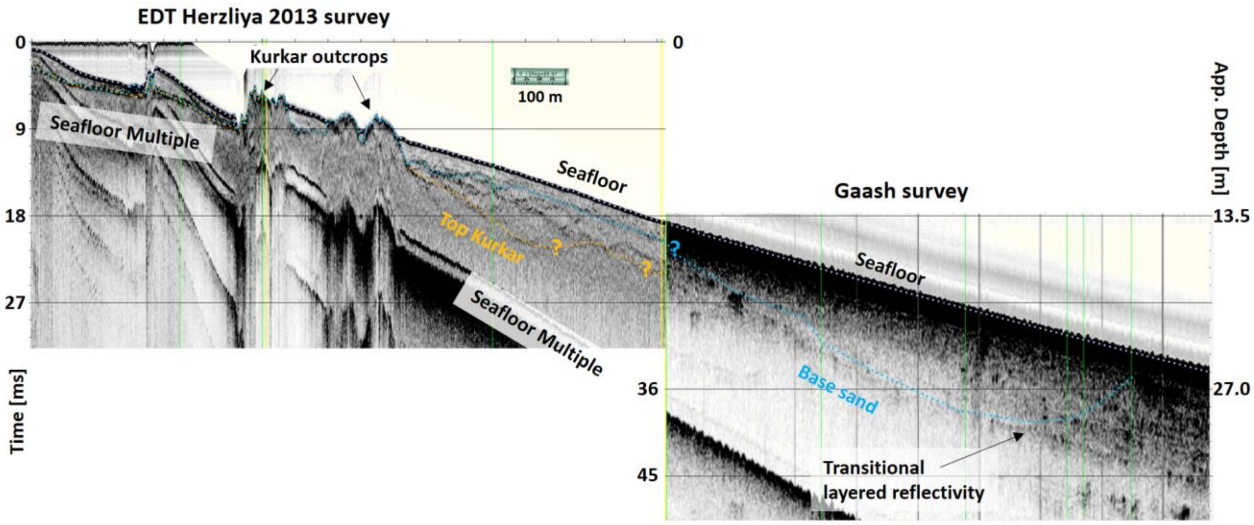

Figure 12. A Chirp sub-bottom profiles composite of the EDT Herzliya 2013 (left) and the Gaash (right) surveys.

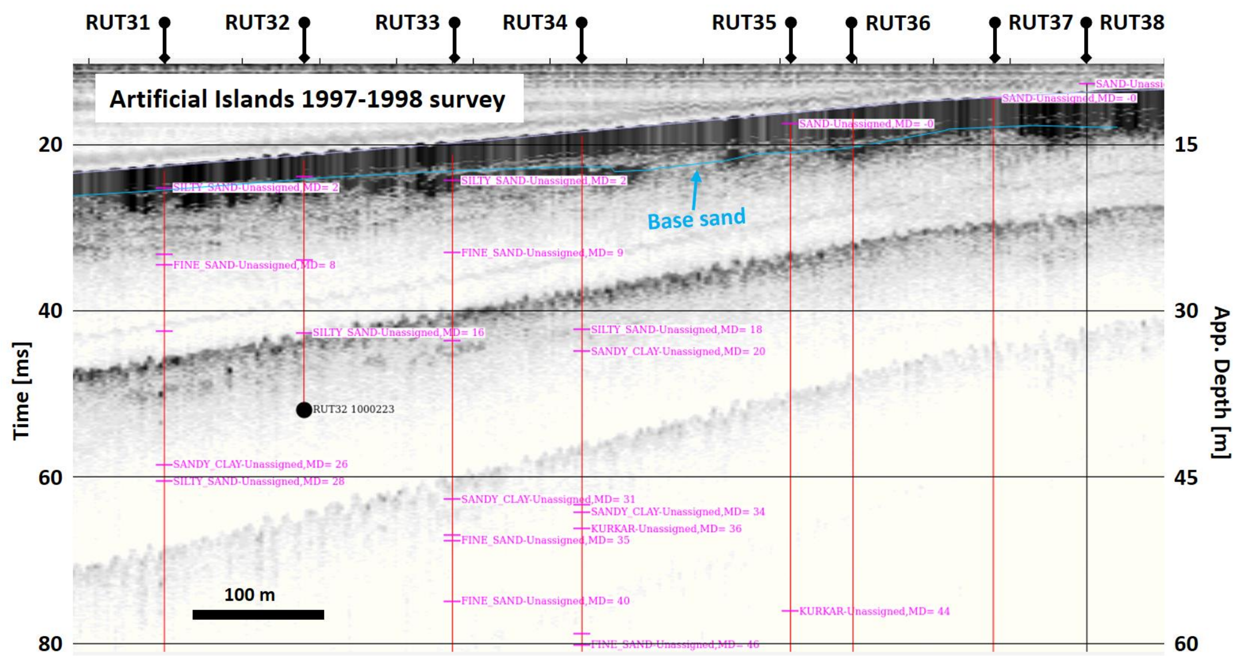

Figure 13. The Chirp sub-bottom profiles of the Artificial Islands 1997-1998 survey aligned with Israel Electrical Company boreholes of Avital (2002) lithological section (figure 3).

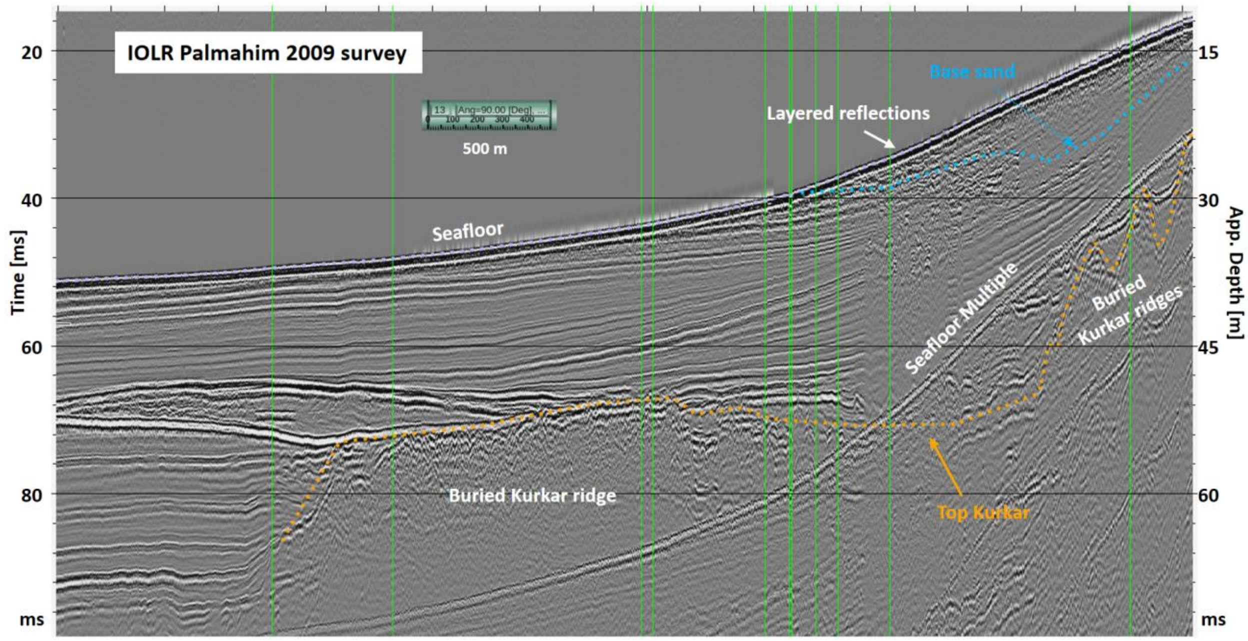

Figure 14. A Sparker sub-bottom profile of the IOLR Palmahim 2009 survey overlaid with the surface interpretations.

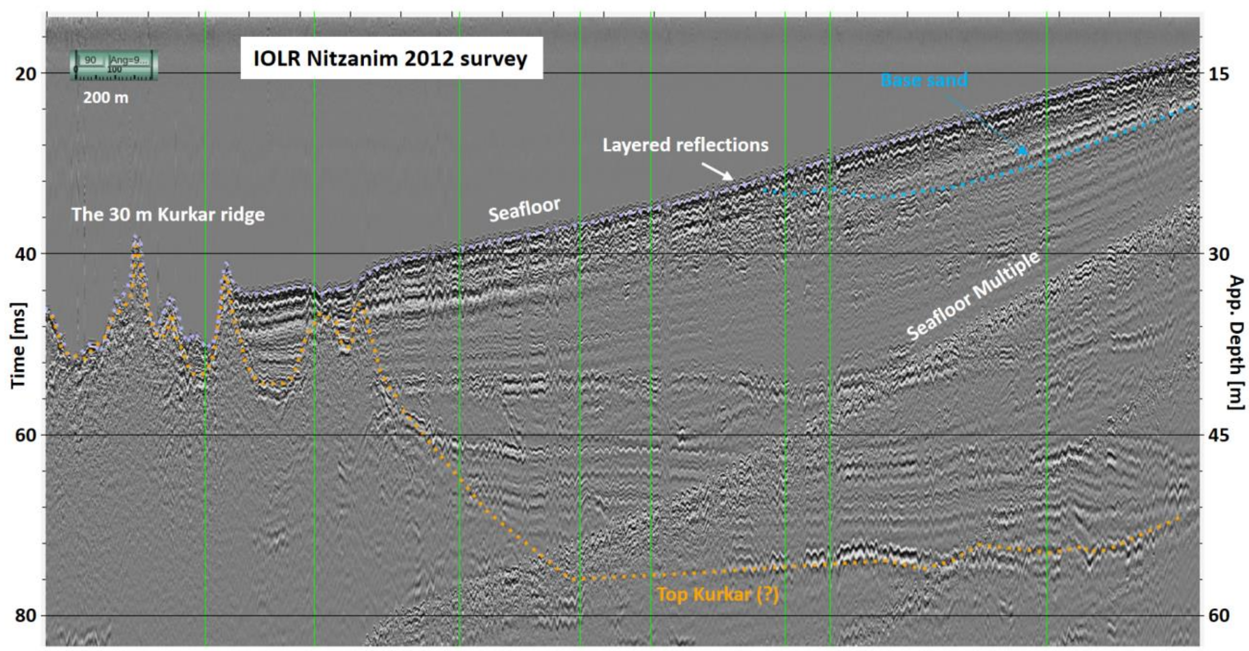

Figure 15. A Sparker sub-bottom profile of the IOLR Nitzanim 2012 survey overlaid with the surface interpretations.

c. Mapping the top of Kurkar and top-most sand unit

Figures 16 and 17 display the actual interpretation picks (left) and the smooth interpolated maps (right) of the depths to the top of Kurkar and base of the top-most sand unit, respectively. The interpretation picks where existing show the details of each of the surfaces, while the picking intervals and gaps depict the level of credibility of the interpolation. The interpolated smoothed maps show the general trends of each of the surfaces, but do not reflect the details.

<u>1. The top of Kurkar:</u>

The top of Kurkar picks (figure 16a) show that this surface is generally well constrained across the northern part of the study area. In contrast from Tel-Aviv southwards there are large gaps, with little control along the nearshore. This difference correlate with the abundance of Kurkar outcrops in the northern part of the study area, particularly along most of the coastline, and the relatively small depths. The interpolated map (figure 16b) shows that the top of Kurkar is generally <6 m beneath the seafloor in the nearshore from Palmahim northward, forming a general ridge along the coastline. To the west of this ridge there is a narrow elongate trough, reaching depths of <15 m below the seafloor and separating the coastline ridge from the 30 m ridge belt. In contrast, in the south part of the study area the top of Kurkar is characterized by a series of oddly shaped ridges and troughs, the latter reaching depths >30 m. Though the details of these structures are ambiguous due to the large data gaps, the presence of such ridges and troughs in the southern part of the study area is well constrained by the data.

<u>2. The top-most sand unit:</u>

The base of the top-most sand unit picks (figure 17a) have a reasonable coverage across the study area in its northern part, but little nearshore coverage to the south of Herzliya. Yet, several interpretation anchors, in the areas of Ashkelon, Port of Ashdod and Palmahim, guarantee that the general trends are robustly delineated by our mapping. In general, the westward extent of these picks define the extent of the top-most sand unit, extending in general to a distance from the coastline of <2.5 km to water depths <30 m. Exceptionally, between Netanya and Hadera the top-most sand unit extends locally to water depths up to 39 m, up to 2.7 km from the coastline. In contrast to the top of Kurkar, the interpolated thickness map of the top-most sand unit reveals little difference between the southern and northern parts of the study area. The sand unit is mostly concentrated along a thin (~1 km wide) elongate generally 4-7 m thick set of slivers, extending sub parallel to the coastline along most of the study area. Between Ashdod and Tel Aviv the sliver is particularly thick, reaching a thickness of up to ~14 m. Outside this set of slivers the sand unit is generally <3 m thick. From Tel-Aviv southward the sand sliver is centered ~1-1.5 km from the coastline, while from Herzliya northward the set of slivers is shifted westward to be centered ~1.5-2 km from the coastline. Integrating the volume of the top-most sand layer along the survey area coast (figure 18) demonstrates that the majority of the sand is stored in this layer at a distance of ~1-2 km from the coastline. The total the volume of the top-most sand unit in the study area is ~700 million m^3, out of which ~450 million m^3 are concentrated within the sand slivers and ~100 million m^3 are concentrated in the exceptionally (>7 m) thick sliver.

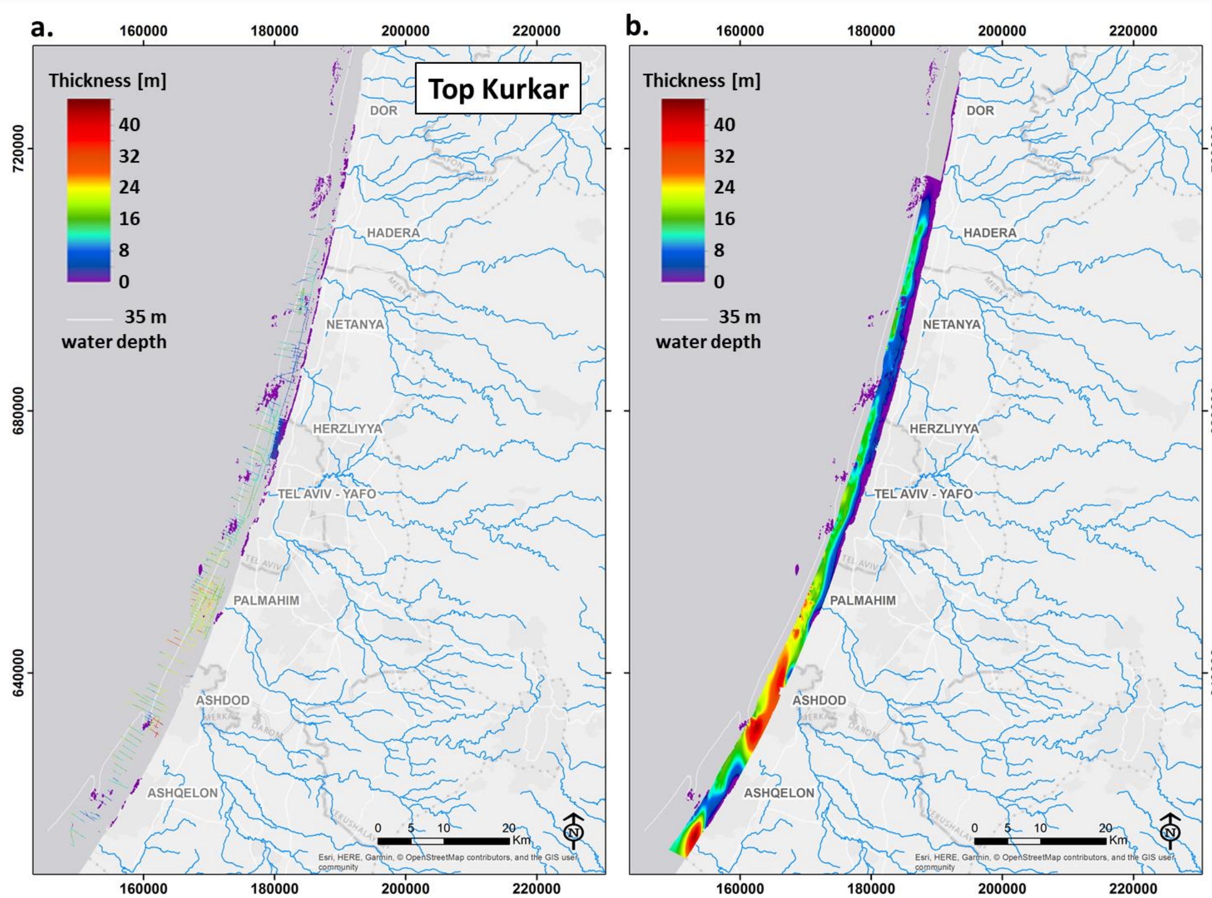

Figure 16. The top of Kurkar depth beneath the seafloor picks (a) and final interpolated map (b).

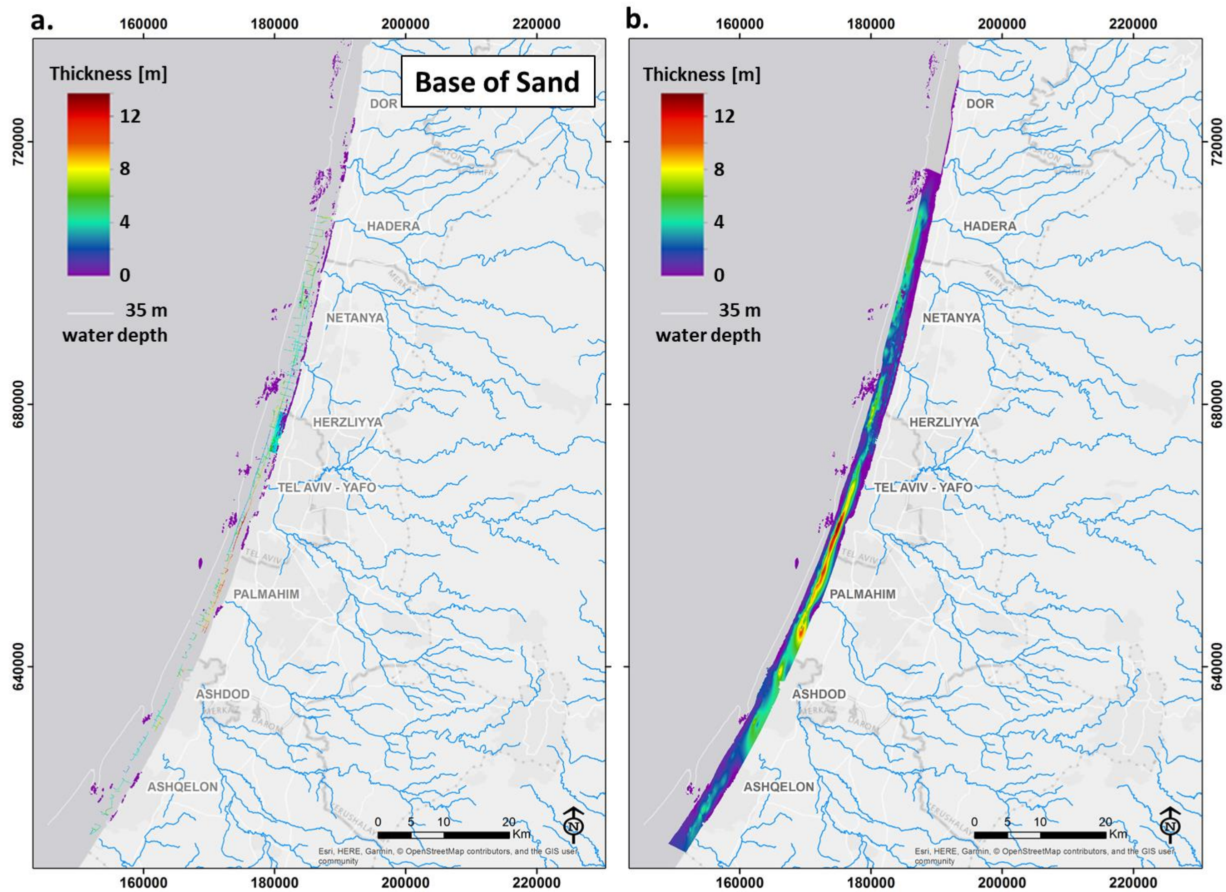

Figure 17. The base of the top-most sand unit depth beneath the seafloor picks (a) and final interpolated map (b).

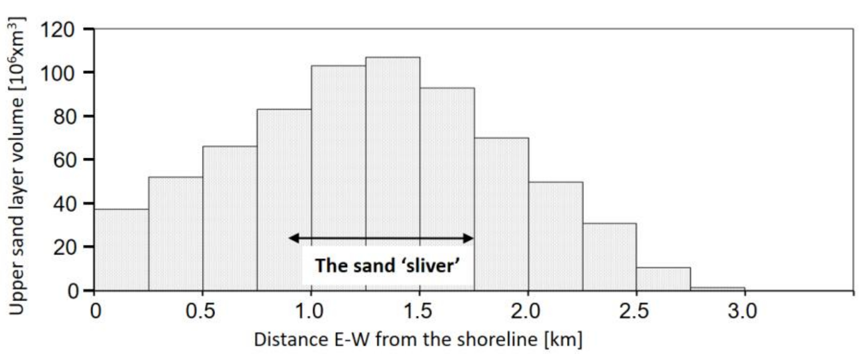

Figure 18. The top-most sand layer volume, integrated along the coast in the survey area, as a function of the distance from the coastline. The generalized outline of the sand slivers is marked.

Conclusions

- The top most sand layer in the research area is a several meters thin layer, with the sand volume concentrated primarily in a set of thin slivers 1.5-2 km from the coastline.
- The total sand volume in the top most layer in the research area is ~$700x10^6$ m^3, out of which ~$450x10^6$ m^3 are concentrated in the sand slivers.
- The distribution of grain sizes reveals that the majority of the sand in this layer is characterized with D50 of ~0.15 mm (and certainly less than 0.2 mm).

Acknowledgements

Funding for this study was granted by The Mediterranean Coastal Cliff Preservation Government Company Ltd. We thank the following for their valuable help in obtaining the datasets incorporated into this study: Roni Nehoray, The Mediterranean Coastal Cliffs Preservation Governmental Company Ltd.; Ahuva Almogi-Labin and John Hall, The Geological Survey of Israel; Eldad Levi, Jean Steinberg and Uri Frieslander, The Geophysical Institute of Israel; Barak Herut, Mor Kanari and Arik Golan, Israel Oceanographic and Limnological Research (IOLR); Gilad Shtienberg, University of Haifa; Rani Amir and Mayan Haim, Israel Ministry of Environmental Protection; Elya Rubinov, Tel Aviv-Yafo Municipality; Paul Vital, Municipality of Netanya; Tamir Frydenrych and Haim Cohen, Marteam Ltd.; Daniela Ostrovsky and Orna Gobernik, Israel Ports Development and Assets Company Ltd.; Israel Planning Administration. We thank Taylor and Francis and Elsevier for permitting the reproduction of figures 1 and 3, respectively, in this report. We thank Paradigm for sponsorship of their software.

References

Avital, A., 2002. Geological History of the Plio-Pleistocene-Holocene offshore based on cores of Askelon, southern Israel. *M.Sc. Thesis, Dep. Of Geology and Environmental Sciences, Ben-Gurion University of the Negev, Israel*, pp. 180 (in Hebrew with English abstract).

Almagor G, Gill D, Golik A, 1998. Artificial Islands Project, geotechnical tests of vibracores. *Israel Geological Survey, Jerusalem, Report GSI/98/28*: 43 p.

Almagor, G., Gill, D. and Perath, I., 2000. Marine sand resources offshore Israel. *Marine georesources & geotechnology*, *18*(1), pp.1-42.

Almagor, G., and Perath, I., 2012. The Mediterranean Shore of Israel. *Geological Survey of Israel Current Research*, *Report No. GSI/28/2012*, pp. 438 (in Hebrew).

Almogi-Labin, A., Calvo, R., Elyashiv, H., Amit, R., Harlavan, Y., and Herut, B., 2012. Sediment characterization of the Israeli Mediterranean shelf. *GSI Report GSI/27/2012 and IOLR Report H68/2012*, 33 p. (in Hebrew with English abstract).

Almogi-Labin, A., Herut, B., Sandler, A., and Gelman, F., 2009. Rapid changes along the Israeli Mediterranean coast following the damming of the Nile and their influence on the Israeli inner shelf. *GSI Report GSI/36/2009 and IOLR Report H75/2009*, 24 p. (in Hebrew with English abstract).

DHV, 2011. New container terminal Ashdod port – Geotechnical investigation report.

Emery, K.O. and Neev, D., 1960. *Mediterranean beaches of Israel*. State of Israel, Ministry of Agriculture, Division of Fisheries, the Sea Fisheries Research Station.

Engelmann, A., Neber, A., Frechen, M., Boenigk, W. and Ronen, A., 2001. Luminescence chronology of upper Pleistocene and Holocene aeolianites from Netanya South—Sharon coastal plain, Israel. *Quaternary Science Reviews*, *20*(5-9), pp.799-804.

Frechen, M., Dermann, B., Boenigk, W. and Ronen, A., 2001. Luminescence chronology of aeolianites from the section at Givat Olga—Coastal Plain of Israel. *Quaternary Science Reviews*, *20*(5-9), pp.805-809.

Frechen, M., Neber, A., Dermann, B., Tsatskin, A., Boenigk, W. and Ronen, A., 2002. Chronostratigraphy of aeolianites from the Sharon Coastal Plain of Israel. *Quaternary International*, *89*(1), pp.31-44.

Fugro Engineers B.V., 1998, Geotechnical survey offshore sand resources of Israel, *Fugro Report No. N-3607/01*.

Goff, J.A., Austin Jr, J.A. and Goodman-Tchernov, B.N., 2018. Estuarine development and early Holocene transgression across an aeolianite substrate, Caesarea, central Israel. *Continental Shelf Research*, *158*, pp.33-44.

Goldsmith, V. and Golik, A., 1980. Sediment transport model of the southeastern Mediterranean coast. *Marine Geology*, *37*(1-2), pp.147-175.

Golik A, 1993. Indirect evidence for sediment transport on the continental shelf off Israel. *Geo-Marine Letters*, 13: 159-164.

Golik, A., 2002. Pattern of sand transport along the Israeli coastline. *Israel Journal of Earth Sciences*, *51*.

Golik A, Gardosh M, Gill D, Almagor G, 1999. Artificial Islands Project – prospection for offshore aggregates. *Israel Oceanographic and Limnological Research, Haifa, Report H19/99*: 31 p and appendices.

Gvirtzman, G., Martinotti, G.M., Moshkovitz, S. and Van Couvering, J.A., 1997. Stratigraphy of the Plio-Pleistocene sequence of the Mediterranean coastal belt of Israel and its implications for the evolution of the Nile Cone. *The Pleistocene Boundary and the Beginning of the Quaternary*, *41*, p.156.

Gvirtzman, G., Netser, M. and Katsav, E., 1998. Last-Glacial to Holocene kurkar ridges, hamra soils, and dune fields in the coastal belt of central Israel. *Israel Journal of Earth Sciences*, *47*(1), pp.27-46.

Gvirtzman, G., Shachnai, E., Bakler, N. and Ilani, S., 1984. Stratigraphy of the Kurkar Group (Quaternary) of the coastal plain of Israel. *Geological Survey of Israel Current Research*, pp.70-82.

Hecht A, 1964. On the turbulent diffusion of the water of the Nile floods in the Mediterranean Sea. Sea. *Fisheries Research Station, Haifa, Bulletin* 36: 1-24.

Hyams-Kaphzan, O., Almogi-Labin, A., Sivan, D. and Benjamini, C., 2008. Benthic foraminifera assemblage change along the southeastern Mediterranean inner shelf due to fall-off of Nile-derived siliciclastics. *Neues Jahrbuch für Geologie und Paläontologie-Abhandlungen*, *248*(3), pp.315-344.

Inman, D.L. and Jenkins, S.A., 1984. The Nile littoral cell and man's impact on the coastal littoral zone in the SE Mediterranean. In *Proceedings of the 17th International Coastal Engineering Conference* (pp. 1600-1617). Sydney, Australia: ASCE.

Jan De Nul Group, 2017. Israel – Askelon_Netanya – 2017_10 – Sand supply and beach reclamation: Piston sampling campaign Ashdod, 13 p.

Katz, T. and Crouvi, O., 2018. Sediment flux dynamics over the shallow (25 m depth) shelf of the Mediterranean Sea along the Israeli coast. *Marine Geology*, *406*, pp.1-11.

Katz, O., Hecht, H., Petranker, G., Almog, E., 2007. Retreat rate of the Israeli coastal cliff and its estimated location at 2100. *Geological Survey of Israel, Report: GSI/21/07* (in Hebrew, abstract in English).

Katz, O. and Mushkin, A., 2013. Characteristics of sea-cliff erosion induced by a strong winter storm in the eastern Mediterranean. *Quaternary Research*, *80*(1), pp.20-32.

Levin, A., Sladkevich, M., Glozman, M., Khudyakova, V., Kit, E., 2011, Netanya coast and cliff protection: hydrographic conditions and marine sediment characteristics. *CAMERI Interim Report P.N.746/11, in: Leshem Sheffer Environmental Quality Ltd., Plan 408-0153510, Netanya coastal cliff preservation stage A. – Sironit Argaman segment: Environmental impact assessment*, 135 p.

Mauz, B., Hijma, M.P., Amorosi, A., Porat, N., Galili, E. and Bloemendal, J., 2013. Aeolian beach ridges and their significance for climate and sea level: Concept and insight from the Levant coast (East Mediterranean). *Earth-Science Reviews*, *121*, pp.31-54.

Mivdaka – Building and Infrastructure Testing Laboratory Ltd., 2013. Herzliya sea front Urban Construction Program (TABA), sub-surface survey, laboratory tests. *Report presented to Marteam Ltd., in: Amir, D. and Karniel, Z., 2016. Environmental Impact assessment, plan no. 504-0467118 (הר/2202)*, 49 p.

Mushkin, A., Katz, O., Crouvi, O., Alter, S.R. and Shemesh, R., 2016. Sediment contribution from Israel's coastal cliffs into the Nile's littoral cell and its significance to cliff-retreat mitigation efforts. *Engineering Geology*, *215*, pp.91-94.

Neev, D., Bakler, N., and Emery, K.O., 1987. Mediterranean Coasts of Israel and Sinai: Holocene Tectonicsm from Geology, Geophysics, and Archaeology. Taylor & Francis.

Neev, D., Edgerton, H.E., Almagor, G. and Bakler, N., 1966. Preliminary results of some continuous seismic profiles in the Mediterranean shelf of Israel. *Isr. J. Earth Sci*, *15*, pp.170-178.

Nir, Y., 1977. Report currently missing.

Nir, Y., 1982. Offshore artificial structures and their influence on the Israel and Sinai Mediterranean beaches. In *Coastal Engineering 1982* (pp. 1837-1856).

Nir YA. Recent sediments of the Israel Mediterranean continental shelf and slope. *Ph.D. Thesis, Department of Marine Geology*, *University of Gothenburg, Sweden,* 149 p.

Nir, Y., Kurkar cliffs in the Mediterranean shores of Israel. *Geological Survey of Israel Current Research*, *Report No. GSI/28/92* , 75 p. (in Hebrew).

Perath I, 1982. Rate of retreat of the Sharon escarpment – a new method of measurement. *In* Ehrlich A, Katz B (editors), Israel Geological Survey, Current Research 1982: 62-65.

Perlin, A. and Kit, E., 1999. Longshore sediment transport on Mediterranean coast of Israel. *Journal of Waterway, Port, Coastal, and Ocean Engineering*, *125*(2), pp.80-87.

Pomerancblum, M., 1966. The distribution of heavy minerals and their hydraulic equivalents in sediments of the Mediterranean continental shelf of Israel. *Journal of Sedimentary Research*, *36*(1), pp.162-174.

Porat, N., Avital, A., Frechen, M. and Almogi-Labin, A., 2003. Chronology of upper Quaternary offshore successions from the southeastern Mediterranean Sea, Israel. *Quaternary Science Reviews*, *22*(10-13), pp.1191-1199.

Porat, N., Wintle, A.G. and Ritte, M., 2004. Mode and timing of kurkar and hamra formation, central coastal plain, Israel. *Israel Journal of Earth Sciences*, *53*(1).

Shoshany, M., Golik, A., Degani, A., Lavee, H. and Gvirtzman, G., 1996. New evidence for sand transport direction along the coastline of Israel. *Journal of Coastal Research*, pp.311-325.

Shtienberg, G., Dix, J., Waldmann, N., Makovsky, Y., Golan, A. and Sivan, D., 2016. Late-Pleistocene evolution of the continental shelf of central Israel, a case study from Hadera. *Geomorphology*, *261*, pp.200-211.

Sivan, D. and Almogi-Labin, A., 1999. Environmental/ecological characterization of sediments and microfauna of the inner shelf offshore, Israel. *Earth Sciences Administration, Ministry of Energy and Natural Resources, State of Israel, Report ES/32/99*, 41 pp. (In Hebrew).

Sivan, D. and Porat, N., 2004. Evidence from luminescence for Late Pleistocene formation of calcareous aeolianite (kurkar) and paleosol (hamra) in the Carmel Coast, Israel. *Palaeogeography, Palaeoclimatology, Palaeoecology*, *211*(1-2), pp.95-106.

Sivan, D., Eliyahu, D. and Raban, A., 2004. Late Pleistocene to Holocene wetlands now covered by sand, along the Carmel Coast, Israel, and their relation to human settlement: an example from Dor. *Journal of Coastal Research*, pp.1035-1048.

Soil and Roads Laboratory, Technion Research and Development Foundation, 1993. Ashkelon-Rutnberg power station sea boring report, Project 5408/93.

Spier, V., and Ben-Yosef, V., 2016a. Monitoring of the marine and coastal environment: “Rotenberg” power plants site, V.A.D. seawater desalination facility, Mekorot wells desalination facilities, Dorad power plant, 2016 report. *Israel Electrical Company Ltd. Report RELP-2-2017*, 318 p.

Spier, V., and Ben-Yosef, V., 2016b. Monitoring of the marine and coastal environment: “Orot Rabin” power plants site, H_2ID seawater desalination facility, 2016 report. *Israel Electrical Company Ltd. Report RELP-3-2017*, 99 p.

Stadler, L., Berent, E. and Zwamborn, J.A., 1996. Breakwater damage due to unique seabottom changes. In *Advances in coastal structures and breakwaters* (pp. 142-157). Thomas Telford Publishing.

Tzadok, R., 2018. The distribution of seafloor grain size between Ashdod port and Ashdod marina, water depths 8-20 meters (sampling quality control). *Report submitted to MCCP*.

Wentworth, C.K., 1922. A scale of grade and class terms for clastic sediments. *The journal of geology*, *30*(5), pp.377-392.

Zviely, D., Kit, E. and Klein, M., 2007. Longshore sand transport estimates along the Mediterranean coast of Israel in the Holocene. *Marine Geology*, *238*(1-4), pp.61-73.